

Distinct Inhibition Modes of New Delhi Metallo- β -lactamase-1 Revealed by NMR Spectroscopy

Kai Cheng, Qiong Wu, Chendie Yao, Zhaofei Chai, Ling Jiang, Maili Liu, and Conggang Li*



Cite This: *JACS Au* 2023, 3, 849–859



Read Online

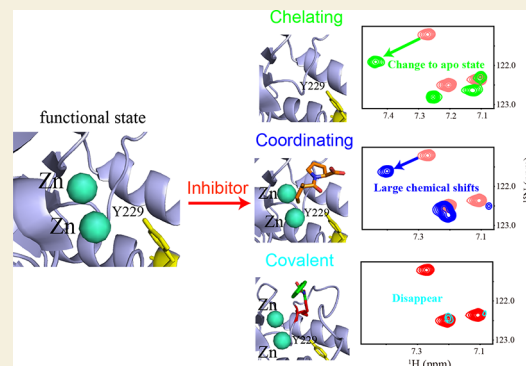
ACCESS |

Metrics & More

Article Recommendations

Supporting Information

ABSTRACT: The wide spread of antibiotic-resistant “superbugs” containing New Delhi metallo- β -lactamase-1 (NDM-1) has become a threat to human health. However, clinically valid antibiotics to treat the superbugs’ infection are not available now. Quick, simple, and reliable methods to assess the ligand-binding mode are key to developing and improving inhibitors against NDM-1. Herein, we report a straightforward NMR method to distinguish the NDM-1 ligand-binding mode using distinct NMR spectroscopy patterns of apo- and di-Zn-NDM-1 titrations with various inhibitors. Elucidating the inhibition mechanism will aid the development of efficient inhibitors for NDM-1.



KEYWORDS: NDM-1, inhibitor, NMR spectroscopy, titration, ligand binding, inhibition modes

INTRODUCTION

The overuse of antibiotics has led to antibiotic-resistant “superbugs”, which have emerged as a threat to public health. The superbugs use β -lactamases to catalyze the opening of the β -lactam rings of antibiotics to make them ineffective. There are four classes of β -lactamases (A, C, D, and B) based on their amino acid sequences.^{1,2} The classes A, C, and D belong to serine- β -lactamases (S β LS) and use an active site serine as the nucleophile for hydrolysis.^{3,4} Class B requires one or two zinc ions (Zn(II)) in the catalysis center for their activity. New Delhi metallo- β -lactamase-1 (NDM-1) belongs to the Class B metallo- β -lactamase (M β L) superfamily and utilizes two zinc ions to catalyze the hydrolysis reaction.⁵

NDM-1 has spread worldwide since its discovery in 2008.^{6–8} NDM-1 confers enteric bacteria with nearly full resistance to almost all β -lactam-containing antibiotics, including the last resorted carbapenems such as meropenem and imipenem.^{9,10} About 190 NDM-1 crystal structures are available in the Protein Data Bank (PDB), including variants, without metal ions, complexed with metal ions and substrates, hydrolysis products, and inhibitors. The NDM-1 structure is a typical $\alpha\beta/\beta\alpha$ sandwich fold of MBLs.^{11,12} Each NDM-1 binds to two divalent zinc ions with different affinities. The two zinc ions are bridged by a water molecule. The first zinc (Zn1) and second zinc (Zn2) are coordinated by His120, 122, 189 and Asp124, Cys208, His250, respectively.^{11–14} The active site of NDM-1 is defined by a hydrophobic cavity, which is quite open and delimited by several flexible loops. NDM-1 has five active site loops (ASL1–ASL5), which are located in shallow grooves at the bottom of the $\beta\beta$ sandwich. These loops, which surround

the catalytic cavity, act as the ceiling, door, and the doorkeeper to close the site during substrate binding and open it for product release.^{11,15} Movements in ASL1 and ASL4 in the active site are considered to be essential for the substrate/inhibitor binding.^{11,13,16} The hydrophobic residues (Leu65, Met67, Phe70, and Val73) in ASL1 are supposed to have hydrophobic interactions with substrates.^{11,14} ASL4 includes residues Cys208, Lys211, and Asn220 that coordinate with Zn2 and interact with the carboxyl group of the substrate.^{11,14}

Many compounds have been clinically used to inhibit serine- β -lactamase,^{17–22} but few of them effectively inhibit metallo- β -lactamase. More than 500 NDM-1 inhibitors have been developed.^{23–25} These inhibitors can be divided into three large groups based on the action mechanism: (i) metal chelating inhibitors (aspergillomarasmine A²⁶ and other natural products) or metalodrugs that replace the zinc ions with other metal ions (auranofin²⁷ and colloidal bismuth subcitrate²⁸), (ii) metal coordinating or binding inhibitors (captopril,²⁹ tiopronin,³⁰ boronic acid derivatives,³¹ and other thiol-containing compounds³⁰), and (iii) covalent inhibitors (ebselen³² and chloromercuribenzoic acid³³). The first kind of inhibitors sequester the zinc ions, acting as chelating agents.

Received: November 30, 2022

Revised: February 13, 2023

Accepted: February 14, 2023

Published: February 27, 2023



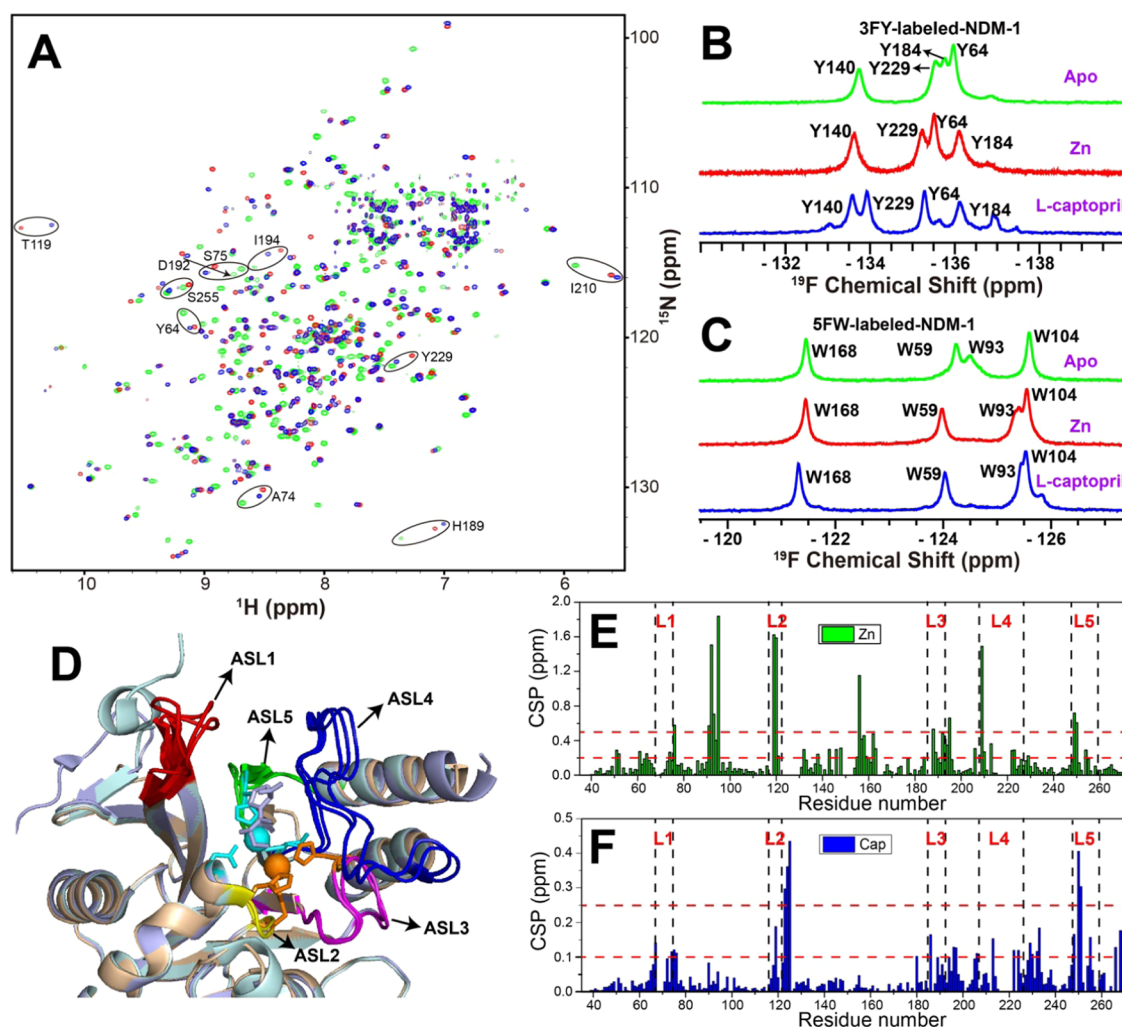


Figure 1. ^1H - ^{15}N TROSY-HSQC spectra and ^{19}F spectra of NDM-1. The overlapped ^1H - ^{15}N TROSY-HSQC spectra of di-Zn-NDM-1 (red), apo-NDM-1 (green), and L-captopril-bound di-Zn-NDM-1 (blue) are shown in A. The ^{19}F spectra of 3FY-labeled- and 5FW-labeled NDM-1 are shown in (B) and (C). The overlapping X-ray structures of di-Zn-NDM-1 (PDB: 3SPU, pale green) with apo-NDM-1 (PDB: 3SBL, pale cyan) and L-captopril-bound di-Zn-NDM-1 (PDB: 4EXS, light blue) are shown in D and the active site loops (ASL1-ASL5) are also labeled in D. The zinc ions are shown in (E) and (F), respectively. Assignments for backbone were obtained using TROSY-HNCACB, TROSY-HN(CO)CACB, and TROSY-HNCA experiments for $^2\text{H}/^{13}\text{C}/^{15}\text{N}$ -labeled apo-NDM-1 and di-Zn-NDM-1. The assigned spectrum of apo-NDM-1 is shown in Figure S1. The assigned spectrum of di-Zn-NDM-1 is shown in Figure S2 [BMRB access code: 27043]. Assignments for ^{19}F spectra were obtained by single point mutation and are shown in Figure S3.

The second kind of inhibitors coordinate the zinc ions and prevent antibiotics from entering. The third kind of inhibitors covalently bind to NDM-1 and irreversibly inhibit NDM-1. Despite the urgent need for broad-spectrum NDM-1 inhibitors, no clinically useful inhibitors have been available till now. Moreover, many clinical variants of NDM have been identified.³⁴ These variants show higher Zn(II) binding affinity, stability, and catalytic activity.^{35,36} However, the inhibitor binding affinity difference for these variants has not been characterized. Solution NMR and other techniques have identified more than 500 compounds that could bind to NDM-1 or inhibit its activity.²³ However, most of them reported no detailed information such as binding sites, binding constant, and inhibition mechanisms, which are critical to optimize or design highly specific and efficient inhibitors. The crystal structures of different functional states bound with inhibitors could provide the molecular mechanism at very high resolution, while obtaining the co-crystal of NDM-1 with the

inhibitor is challenging and time consuming. Solution NMR has been widely used to investigate protein–ligand interactions. The ligand-based techniques such as water-LOGSY, STD, and NOE-pump have been used for high-throughput screening.^{37–45} Protein-based NMR could confirm the hits by ligand-based NMR and provide a more detailed binding mode and inhibition mechanism. Rydzik et al. have used ^{19}F NMR to monitor the conformational changes of NDM-1 upon substrate binding.^{46,47} However, the detailed binding sites, affinity, and action mode are difficult to obtain from one ^{19}F labeling site. Rivière et al. have studied the interactions of several flavonols with NDM-1 using NMR spectroscopy and identified the binding sites on NDM-1.⁴⁸ Palica et al. have also utilized NMR spectroscopy to determine the binding sites of phosphonamide monoesters on NDM-1.⁴⁹ Here we explore the protein-based NMR technique to elucidate the inhibition mechanisms of NDM-1 inhibitors and quantitatively characterize the binding affinities of inhibitors.

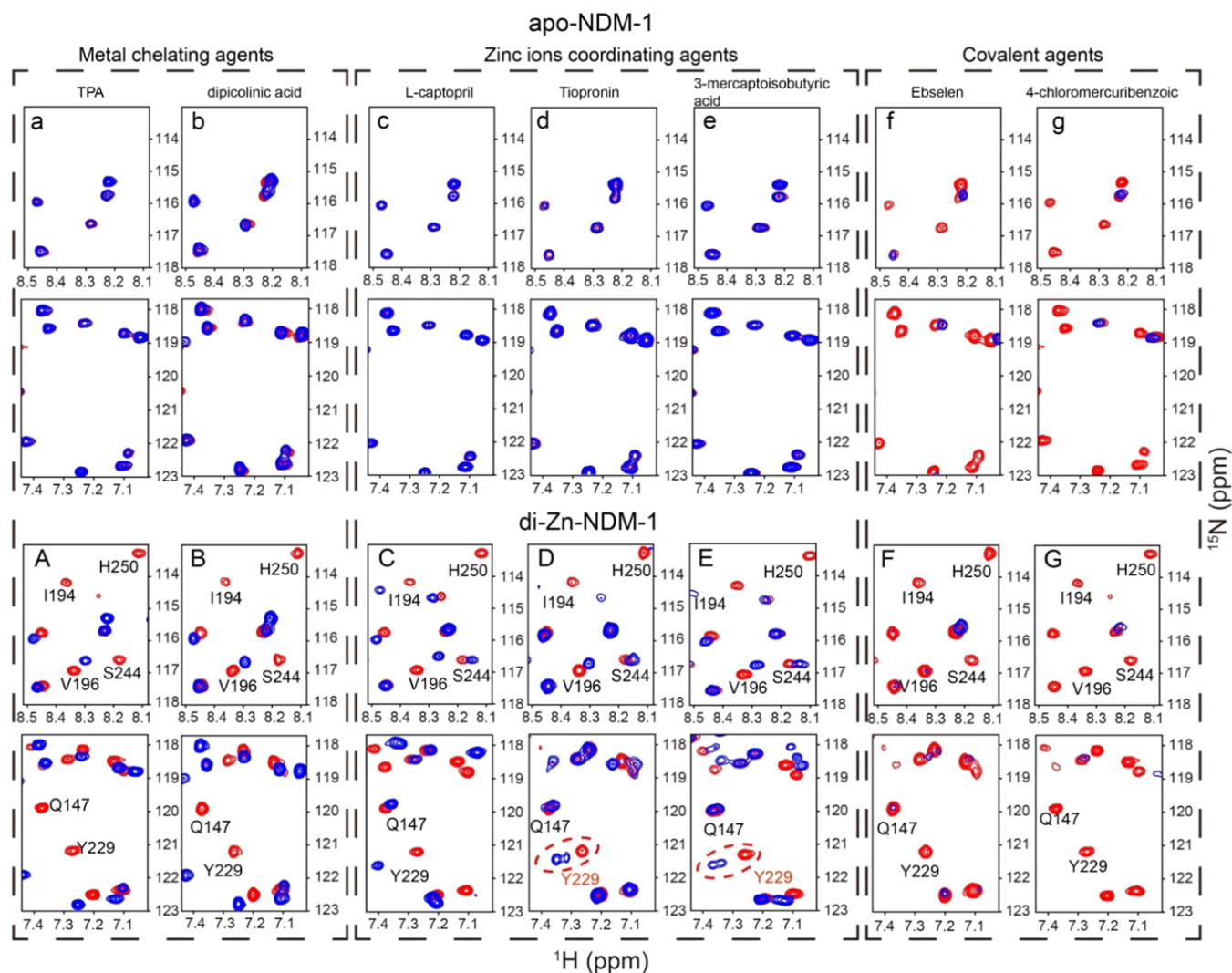


Figure 2. ^1H - ^{15}N TROSY-HSQC spectra of apo-NDM-1 (a–g) (Red) and di-Zn-NDM-1 (A–G) (Red) titrated with inhibitors (blue); TPA (A, a), dipicolinic acid (B, b), L-captopril (C, c), tiopronin (D, d), 3-mercaptopisobutyric acid (E, e), ebselen (F, f), and 4-chloromercuribenzoic acid (G, g). Two cross-peaks are observed for Y229 when di-Zn-NDM-1 was titrated with tiopronin and 3-mercaptopisobutyric as shown by the circles in (D) and (E), which are probably due to the D-, L-stereoisomers.

RESULTS AND DISCUSSION

2D ^1H - ^{15}N TROSY-HSQC and 1D ^{19}F NMR Spectra Are Sensitive to the Conformational States of NDM-1

The ^1H - ^{15}N TROSY-HSQC spectrum is sensitive to protein conformation and is regarded as a “fingerprint” of a protein, so it can be used to monitor the global changes of a protein and provide detailed information about the binding and hydrolysis mechanisms. Although the crystal structures of apo (apo-NDM-1), functional NDM-1 (di-Zn-NDM-1), and substrate or inhibitor-bound NDM-1 (L-captopril) are similar (Figure 1D), we found that their ^1H - ^{15}N TROSY-HSQC spectra and ^{19}F spectra are quite different (Figure 1A–C).

We assigned the backbone resonances of apo and functional NDM-1 (Figures S1 and S2). For apo-NDM-1, 85% backbone amide protons were assigned for non-proline residues. The missing assignments are residues G36–E40, G42, G69, G84, V118, H122–M129, A149–G153, A165, N176, G186, G200, G207, C208, K216, S217, N220, A257, L271, and E272. These residues are mainly located in the flexible loops. Compared with the assignments by Rivière et al.,⁴⁸ several residues

haven't been assigned, probably due to the different experimental conditions. For functional NDM-1, we have improved our previously published assignment⁵⁰ and 96% backbone amide protons were assigned for non-proline residues. Only 9 residues (G36, Q37, G69, A165, G207, K216, S217, L218, and N220) of backbone proton assignments were missing for our results and 14 backbone proton assignments of 14 residues (residues M28–E30, N57, K125, M126, G186, G207, K216, N220, L221, A257, L271, and E272) were missing for the assignments by Rivière et al.⁴⁸ These residues were located in the flexible loops and underwent conformational exchange or fast exchange with water, which induced a significant broadening for cross-peaks. The appearances of the ^1H - ^{15}N TROSY-HSQC spectra of apo-NDM-1 and di-Zn-NDM-1 are almost the same as those in the literature.⁴⁸ Compared with apo-NDM-1, residues in or near active site loops (T119 and H120 in ASL2; G188 ~T195 in ASL3; L209 in ASL4; S249 and H250 in ASL5) that are involved in or near the Zn(II) binding sites and residues in other loops (T91~D95, A156, A157, Q158) show the largest chemical shift variations (larger than 0.5 ppm) for di-Zn-

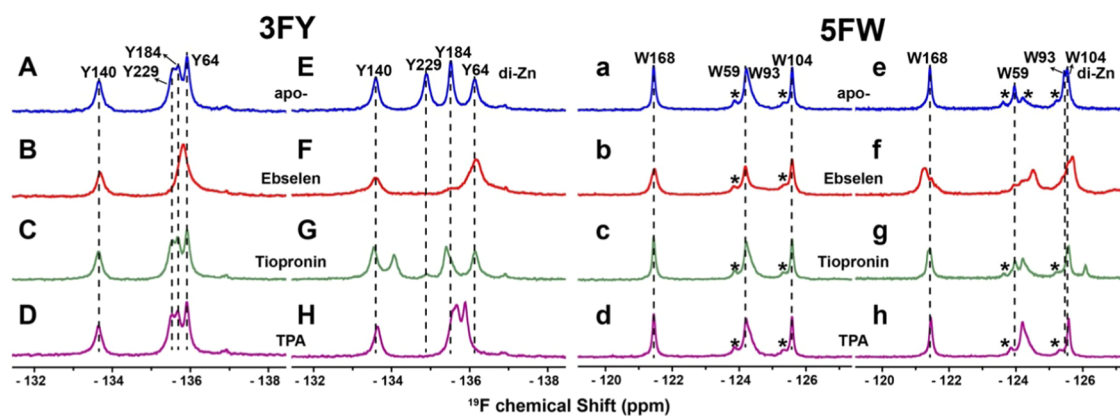


Figure 3. ^{19}F spectra of 3FY-labeled (A–H) and 5FW-labeled (a–h) NDM-1 titrated with ebselen, tiopronin, and TPA; the signals with (*) labeled represent unknown and unassigned peaks. The titration ratios were controlled to ensure the NDM-1 was mostly bound.

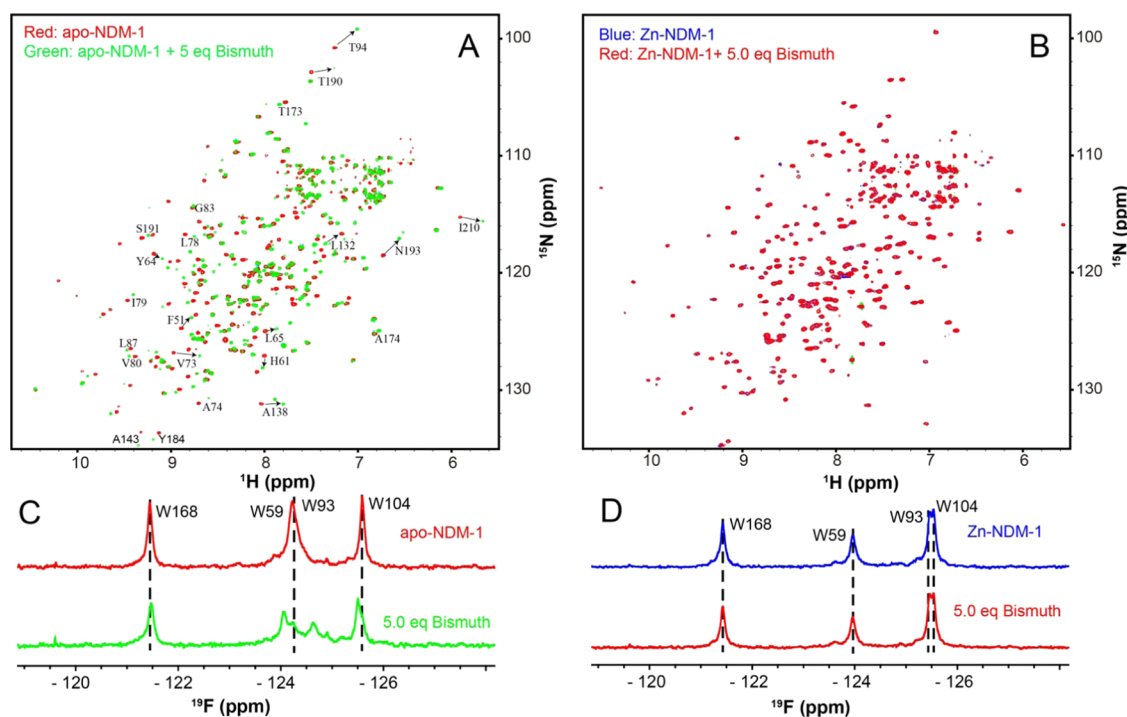


Figure 4. ^1H - ^{15}N TROSY-HSQC spectra and ^{19}F spectra of NDM-1 titrated with CBS. Overlay ^1H - ^{15}N TROSY-HSQC spectra of apo-NDM-1 and di-Zn-NDM-1 titrated with CBS (A, B); ^{19}F spectra of apo-NDM-1 and di-Zn-NDM-1 titrated with CBS (C, D).

NDM-1 in the ^1H - ^{15}N TROSY-HSQC spectra (Figure 1A,E). The active site residues S75 near ASL1 and Y229 in ASL4 also show significant chemical shift differences (larger than 0.2 ppm). We obtained almost the same chemical shift variation patterns between apo-NDM-1 and di-Zn-NDM-1 as Rivière et al. For L-captopril-bound di-Zn-NDM-1, residues (Q123, D124, K125, H250, S251) in or near the Zn(II) binding site show the largest chemical shift perturbations (larger than 0.25 ppm) compared with di-Zn-NDM-1. Larger chemical shift differences (larger than 0.1 ppm) are also observed for residues in or near ASL1 (M67, A72, A74~N76) and ASL4 (Y229, A230, S232, A233) for L-captopril-bound di-Zn-NDM-1.

NDM-1 has four tyrosines (Y64, Y140, Y184, and Y229) and four tryptophans (W59, W93, W104, and W168) that were labeled with 3-fluorotyrosine (3FY) and 5-fluorotryptophan (5FW). We collected the ^{19}F spectra of NDM-1 and then assigned the ^{19}F signals through single point mutation (Figure S3). Three (Y64, Y184, Y229) of four tyrosines and two (W59,

W93) of four tryptophans are sensitive to Zn(II) binding with significant chemical shift differences (about 0.40, 0.42, 0.28, 0.26, and 0.91 ppm, respectively) in ^{19}F spectra between apo- and di-Zn-NDM-1. Residues Y64, Y229, and W93 are also sensitive to L-captopril binding and show large chemical shift perturbations (0.22, 1.28, and 0.40 ppm, respectively) in ^{19}F spectra between di-Zn-NDM-1 and L-captopril-bound di-Zn-NDM-1. These observations indicate that both ^1H - ^{15}N TROSY-HSQC and ^{19}F spectra are sensitive to the different conformational states of NDM-1 and could be used to assess the binding modes between the inhibitors and NDM-1 in the apo-inactive state or di-Zn functional state, respectively.

Distinct Patterns of Spectroscopic Changes in the Presence of Various Inhibitors

We collected the ^1H - ^{15}N TROSY-HSQC and ^{19}F NMR spectra of the ^{15}N -enriched and ^{19}F -labeled NDM-1 titrating with 14 different kinds of inhibitors, including dipicolinic acid,^{S1} tris-

picolylamine (TPA),⁵² auranofin,²⁷ colloidal bismuth subcitrate,²⁸ L-captopril,²⁹ tiopronin,³⁰ thiorphan,³⁰ 3-mercaptopisobutyric acid,⁵³ ebselen,³² 4-chloromercuribenzoic acid,³³ phenanthroline,^{54,55} 2,3-dimercapto-1-propanol,³⁰ dithiothreitol, and cefaclor⁵⁶ (Figures 2, 3 and S5). The structures of these inhibitors are shown in Figure S4. The inhibition mechanisms of these inhibitors are known except for dithiothreitol and can be divided into three groups: (1) inhibitors competitively chelate with Zn²⁺ and deprive the Zn²⁺ of its active site or replace Zn²⁺ with other metals such as bismuth; (2) inhibitors coordinate the Zn²⁺ to block the active site and prevent the substrate from entering; (3) inhibitors chemically react with the side chain and covalently bind to NDM-1 and alter its conformation or stability.

Dipicolinic acid, phenanthroline, and TPA are typical Zn²⁺ chelates. They inactivate NDM-1 by removing its zinc ions, which are essential to its catalytic activity. Upon titration with these agents, the 2D TROSY-HSQC spectra and ¹⁹F spectra of di-Zn-NDM-1 showed significant changes, especially for the residues that bind to or near the Zn²⁺ site, while only minute chemical shift changes were observed for apo-NDM-1 (Figures 2a,b, S5a; 3D,H,d,h). The final titrated spectra for apo- and di-Zn-NDM-1 are the same because the chelators remove the Zn²⁺, the di-Zn-NDM-1 change back to the apo-state, and the chelators themselves do not interact with the apo-NDM-1. Ten equivalent, six equivalent, and fifteen equivalent inhibitors are needed to completely remove the Zn²⁺ from di-Zn-NDM-1 for dipicolinic acid, phenanthroline, and TPA, respectively.

Metalloodrugs that replace the two zinc ions of NDM-1 with other metal ions such as auranofin and colloidal bismuth subcitrate (CBS) have been shown to effectively inhibit NDM-1 activity. We incubated apo-NDM-1 and di-Zn-NDM-1 with CBS and Au(PET₃)Cl at room temperature overnight and recorded the ¹H-¹⁵N TROSY-HSQC and ¹⁹F NMR spectra to evaluate the bindings of bismuth and gold with NDM-1. However, the titrations of Au(PET₃)Cl to NDM-1 lead to protein precipitations. Only the titration of bismuth to NDM-1 is discussed. As shown by the ¹H-¹⁵N TROSY-HSQC and ¹⁹F NMR spectra in Figure 4, the peaks of apo-NDM-1 from residues in or near the active sites (Y64, L65, A74, W93, T94, T190, N193, L209, I210, Y229) shifted significantly when titrated with CBS. The ¹H-¹⁵N TROSY-HSQC and ¹⁹F spectra of di-Zn-NDM-1 showed no changes upon CBS titrations. When titrating bismuth-bound NDM-1 (Bi-NDM-1) with two equivalents Zn²⁺, the ¹H-¹⁵N TROSY-HSQC spectra change back to the active state (Figure S6), which indicates that the bismuth ions fail to replace the zinc ions of di-Zn-NDM-1. Compared with di-Zn-NDM-1, the cross-peaks of residues H120, H122, D124, H189, C208, and H250 that coordinate with the zinc ions in ¹H-¹⁵N TROSY-HSQC spectra for bismuth-bound NDM-1 disappeared. These peaks also disappeared in the ¹H-¹⁵N TROSY-HSQC spectra of apo-NDM-1 and only appeared when the residues coordinated with zinc ions. As shown in Figures S7 and S8, the peaks of Bi-NDM-1 from the residues from or near active sites (Y64, L65, D66, V73, A74, T94, S191-N193, I210) shifted significantly compared with di-Zn-NDM-1, which suggested the localization of bismuth in the active site. These results show that we could utilize ¹H-¹⁵N TROSY-HSQC and ¹⁹F titrations to monitor the bindings of trivalent ion Bi³⁺ with NDM-1.

L-captopril, tiopronin, 3-mercaptopisobutyric acid, 2,3-dimercapto-1-propanol, thiorphan, and dithiothreitol were selected as coordinating agents for titration of NDM-1. The results

(Figures 2C–E, 3C,G,c,g and S5B,C) show large chemical shift changes in ¹H-¹⁵N TROSY-HSQC spectra upon titration of di-Zn-NDM-1. For L-captopril, tiopronin, 3-mercaptopisobutyric acid, 2,3-dimercapto-1-propanol, and dithiothreitol, only two sets of resonances are observed. The chemical shift perturbations upon titration of these inhibitors showed the same binding pattern (Figure S9). The cross-peaks with large CSPs from ALS1 (M67-S75), D90, ALS2 (T119-K125), ALS3 (G186-H189), ALS4 (G206-I210, Y229), and ALS5 (M248-S251) are mainly located in or near the active site. No changes are observed when apo-NDM-1 is titrated with these agents (Figures 2c–e, S5b,c). Thiorphan can easily form intermolecular disulfide bonds in the absence of reductants. For thiorphan titration without TCEP, the cross-peaks shift as the ligand titration ratio increases (Figure S10). The cross-peaks with large chemical shift perturbations (as shown in Figure S10 by the arrows) from T62, F70, V73, A74, D124, K125, H250, S251, and S255 are mainly located in Zn2 binding sites and ALS1. For thiorphan titration in the presence of TCEP, only two sets of resonances are observed (Figure S11). Residues L65, D66, V73, A74, T94, and L209 from active sites show large CSPs. The binding of zinc coordinating agents with di-Zn-NDM-1 involves the zinc ion and amino acids in the active site. The ¹H-¹⁵N TROSY-HSQC spectra remain unchanged for apo-NDM-1. In contrast, the changing pattern is different for di-Zn-NDM-1 when titrating both Zn²⁺ chelating or coordinating agents. We can easily differentiate the binding modes of zinc ions coordinating agents and zinc chelating agents by a simple analysis of the titrated spectra of di-Zn-NDM-1. What's more, when titrated with tiopronin, 3-mercaptopisobutyric acid, and thiorphan, the residues in or near active sites (L65–S75, W93, T94, H189, T190, C208–I210, Y229, A230) show two sets of distinct (Figures 2D, 2E, and S11) peaks probably due to D-, L-stereoisomers.

We chose ebselen, chloromercuribenzoic acid, and cefaclor as covalent inhibitors. To our surprise, almost all of the cross-peaks in the 2D TROSY-HSQC spectra disappear upon titration of apo-NDM-1 and di-Zn-NDM-1 (Figures 2F,G,f,g, and S5D,d). The broadening and disappearance suggest the existence of intermediate chemical exchange on the NMR time scale. Ebselen and 4-chloromercuribenzoic form covalent bonds to the Cys208 side chain, disrupting the coordination of Zn2 and leading to the Zn dissociation from the active site.^{32,33} Cefaclor inhibits NDM-1 with mM affinity and involves Lys211.⁵⁶ The inhibitor forms covalent bonds with amino acid side chains in the active site, which probably disrupts the structural stability of NDM-1. To assess the structural stability of NDM-1 binding with covalent inhibitors, we measured the thermal stability of NDM-1 and ebselen-bound NDM-1 (Figure S12). The *T_m* value of apo-NDM-1 and ebselen-bound apo-NDM-1 is the same (46.1 °C). However, the *T_m* value of ebselen-bound di-Zn-NDM-1 (48.4 °C) is about 5.5 °C lower than that of di-Zn-NDM-1 (53.9 °C), which suggests that the structural stability of NDM-1 decreased upon binding with ebselen. To assess the conformation changes of NDM-1 binding with covalent inhibitors, we collected the ¹⁹F spectra of 3FY- and 5FW-labeled NDM-1 titrated with ebselen. The titration of NDM-1 with ebselen caused significant spectral line broadening in ¹⁹F spectra (Figure 3B,F,b,f), which also suggested the existence of conformational exchange. The ¹⁹F titration spectra of NDM-1 with tiopronin, 3-mercaptopisobutyric acid, DTT, 2,3-dimer-

capto-1-propanol, and TPA are in accordance with the ^1H - ^{15}N TROSY-HSQC spectra.

Assuming that each spectrum is a linear combination of a few basis spectra, principal component analysis (PCA) can be used for the analysis of a series of spectra by singular value decomposition (SVD) analysis. To explore the binding mode of inhibitors with NDM-1 systematically, we performed the PCA to differentiate the binding mode of inhibitors by referring to the method developed by Sakurai and co-workers.⁵⁷ Compared to the covalent inhibitors, both the metal chelators and zinc coordinators titrations showed significant CSPs in the ^1H - ^{15}N TROSY-HSQC spectra of di-Zn-NDM-1. We utilized ^1H and ^{15}N CSPs of 123 traceable residues in the ^1H - ^{15}N TROSY-HSQC spectra of di-Zn-NDM-1 induced by metal chelators (dipicolinic acid, phenanthroline, and TPA) and zinc coordinators (L-captopril, tiopronin, 3-mercaptoprobutyric acid, 2,3-dimercapto-1-propanol, and dithiothreitol) titrations to conduct the PCA. After a singular value decomposition, we succeeded in obtaining 8 components and their corresponding contribution ratios. The contributions of the first two principal components were 77.3 and 7.9%, respectively. The results are shown in Figure 5. We also

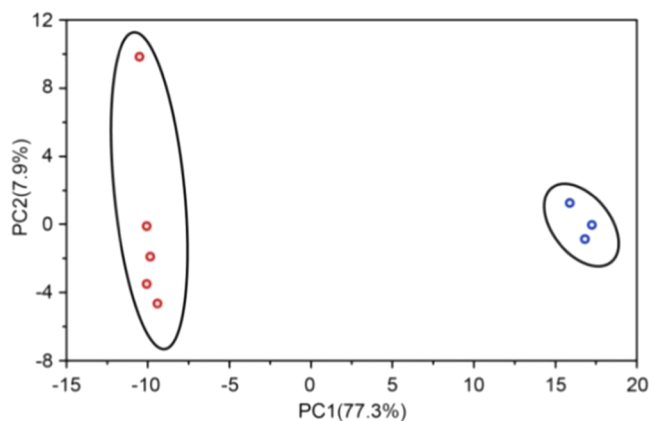


Figure 5. PCA plot of NDM-1 titrated with metal chelators (Blue) and zinc coordinators (Red).

performed the PCA of chemical shift perturbations from 43 residues in the active sites. The result is almost the same as the one using 123 traceable residues. By PCA, we can distinguish different binding modes of inhibitors with NDM-1.

Binding Affinity Measurements of Inhibitors by NMR

The ^1H - ^{15}N TROSY-HSQC and ^{19}F titration spectra is a straightforward method that can detect the ligand binding over a wide affinity range, including very weak interactions ($K_D > 1$ mM). For thiorphan titration without TCEP, the dissociation constants for residues with large CSPs are shown in Figure S13. The dissociation constant for these residues with NDM-1 ranged from 1.9 mM (V73) to 4.5 mM (F70). The binding affinities of DTT, tiopronin, and 2,3-dimercapto-1-propanol with NDM-1 were calculated from the ^{19}F NMR titration data (Figure 6). The dissociation constants calculated from residue Y229 are 30, 121, and 712 μM for DTT, tiopronin, and 2,3-dimercapto-1-propanol, respectively, which are very similar to the results from the ITC experiments (Figure S14).

Differential Affinities of NDM-1 and Clinical Variants

Overuse of antibiotics has led to the evolution of NDM-1 to better recognize new kinds of antibiotics and inhibitors. According to the β -Lactamase DataBase (BLDB)(<http://blpdb.eu/>), 41 different variants of NDM-1 have been identified from infected animals or the clinic with altered antibiotic resistance.³⁴ These variants show altered catalytic activity, thermal stability, substrate selectivity, and Zn binding affinity. However, the effects of mutations on NDM-1 inhibitor binding affinity have rarely been examined, which hinders the development of new inhibitors. In order to investigate the NDM-1 clinical variants' binding affinity with inhibitors, we also titrated di-Zn-NDM-1 and di-Zn-NDM-12 (M154L/G222D) with 3-mercaptoprobutyric acid and calculated the inhibitor affinities through the titrated ^1H - ^{15}N TROSY-HSQC spectra. As shown in Figure S15, the overlapped ^1H - ^{15}N TROSY-HSQC spectra of di-Zn-NDM-12 (M154L/G222D) and di-Zn-NDM-1 only show little differences in residues in or near the mutant sites and active sites, which indicated that the structure of di-Zn-NDM-12 remained unchanged. The peak intensities in the titrated ^1H - ^{15}N

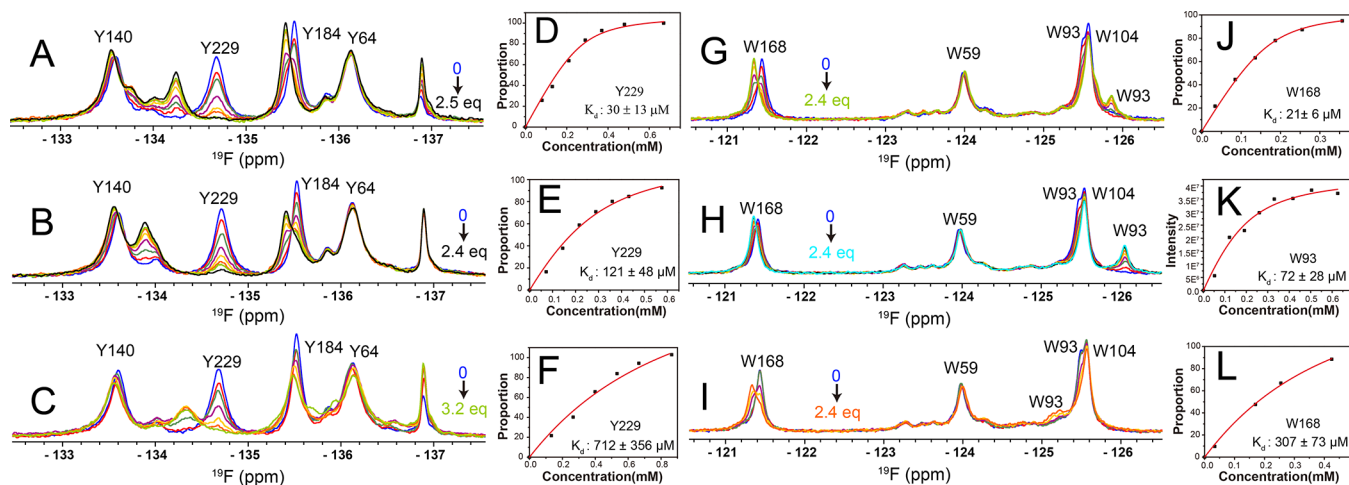


Figure 6. ^{19}F NMR spectra enable the determination of the binding affinity of inhibitors with di-Zn-NDM-1. ^{19}F spectra of 3F_Y-labeled and 5F_W-labeled di-Zn-NDM-1 titrated with DTT (A, G), tiopronin (B, H), and 2,3-dimercapto-1-propanol (C, I). Fitting curves of the dissociation constant for NDM-1 with DTT (D, J), tiopronin (E, K), and 2,3-dimercapto-1-propanol (F, L). The residues selected for the fitting and the dissociation constant are marked in the figure.

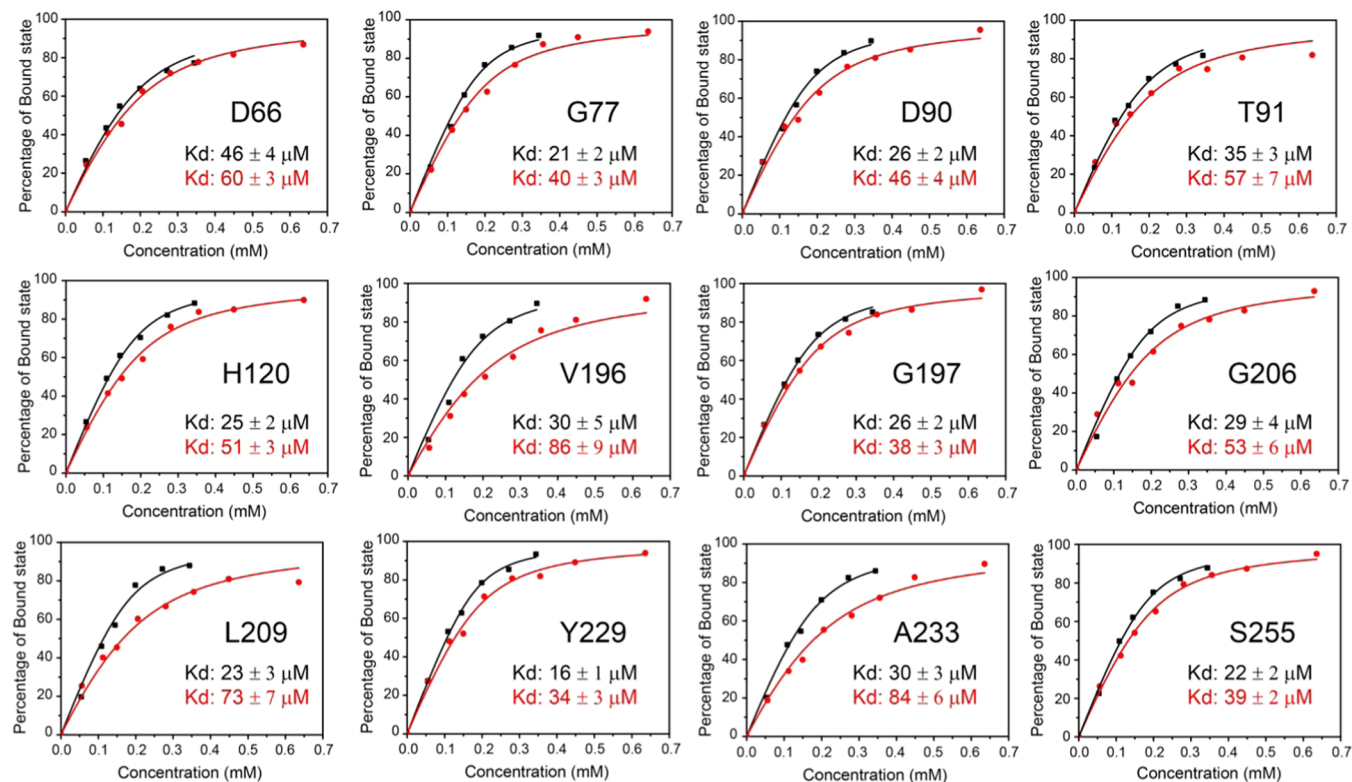


Figure 7. Fitting curves of the dissociation constants of residues D66, G77, T91, H120, V196, G197, D202, G206, L209, I210, A224, and S255 for di-Zn-NDM-1 (black) and di-Zn-NDM-12 (red) with 3-mercaptopisobutyric acid.

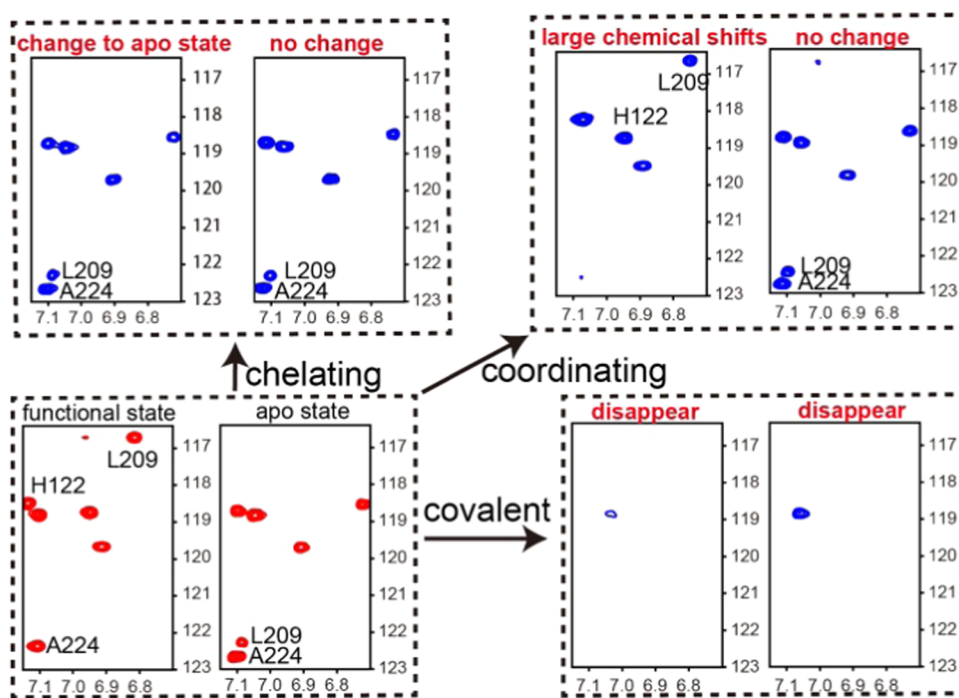


Figure 8. Discriminating inhibition modes by titrating the ^1H - ^{15}N TROSY-HSQC spectra of di-Zn-NDM-1 and apo-NDM-1 with inhibitors.

TROSY-HSQC spectra of bound and unbound states are used to calculate the binding affinity (Figure 7). The binding affinity reduced almost twofold for di-Zn-NDM-12. Compared with di-Zn-NDM-1, the dissociation constants (K_d) increased from 25, 23, 16, and 22 to 51, 73, 34, and 39 μM for residues H120, L209, Y229, and S255, respectively. NDM-12 binds zinc(II)

more tightly than NDM-1 and the affinities for zinc(II) are 6.6 and 18.6 μM , respectively.³⁵ For captopril and its analogues, the thiol moiety of these inhibitors intercalates between the two zinc ions of NDM-1, which squeezes out and displaces the water molecule.⁵⁸ The enhanced Zn2 affinity for NDM-12 may weaken the interaction between Zn2 and the thiol moiety of

coordinating inhibitors, reducing the binding affinity with the coordinating inhibitors. Our results show that the clinical variants of NDM-1 can make the inhibitor less effective than NDM-1 and more attention should be paid to this when developing new inhibitors.

CONCLUSIONS

For all of the 12 inhibitors tested here, we can account for the changes of the ^1H - ^{15}N TROSY-HSQC and ^{19}F spectra of the apo- and di-Zn-state to define their inhibition mode. We conclude that the 2D ^1H - ^{15}N TROSY-HSQC and 1D ^{19}F titration experiments are useful for identifying and distinguishing the inhibition modes (Figure 8). For Zn^{2+} chelators, the di-Zn-NDM-1 spectra change to those of the apo form, but those of the apo-NDM-1 remain the same. For Zn^{2+} coordinators, resonances from the active site have significant chemical shift changes, while the apo-form spectra are unchanged and ^{19}F spectra show the same trend as the 2D TROSY-HSQC spectra. For covalent inhibitors, many resonances disappear in the 2D TROSY-HSQC spectra and the ^{19}F resonances are broadened in the ^{19}F spectra of apo- and di-Zn-NDM-1. However, for Zn^{2+} chelators that deprive $\text{Zn}(\text{II})$ at the active site, it is difficult to selectively chelate $\text{Zn}(\text{II})$ over other metal ions, which are important for human metalloenzymes.⁵⁹ For covalent inhibitors that covalently bind to the side chains of NDM-1, it is hard to achieve specificity over other proteins. Given these reasons, the Zn^{2+} coordinators with high affinity and specificity are the most promising inhibitors that can be developed into clinical drugs. Thus, a high-throughput screen, and rapid distinction and identification of the inhibitors is important for the development of new inhibitors. The ^1H - ^{15}N TROSY-HSQC and ^{19}F spectra can be used to screen and optimize the inhibitors and contribute to drug development.

The ^1H - ^{15}N TROSY-HSQC and ^{19}F titration spectra is a relatively sensitive method and provides a wealth of information about protein–inhibitor interaction, such as binding sites, binding constants, and binding modes, and can detect the ligand binding over a wide affinity range, including very weak interactions ($K_D > 10 \mu\text{M}$). Several NMR studies have been performed to investigate the interactions of NDM-1 with inhibitors.^{48,49,60} Their results all showed large chemical shift variations from the residues in or near the active sites of di-Zn-NDM-1 upon ligand titrations. ^1H NMR spectroscopy has been reported to real-time monitor the NDM-1 activity in living cells.⁶¹ Considering the wide application of ^{19}F NMR in living cells, the ^{19}F NMR titration method might also be exploited to investigate binding in complex environments.

In conclusion, we have shown that a simple ^1H - ^{15}N TROSY-HSQC- and fast ^{19}F -based titration method can be used to accurately assess the NDM-1 inhibition mode. Three different action modes of all of the tested inhibitors were unambiguously revealed. Moreover, quantitative information such as dissociation constants and the residues involving in the binding sites, which are critical for inhibitor design and optimization, can also be determined. Together with the conventional screening methods, the ^1H - ^{15}N TROSY-HSQC and ^{19}F titration method described here can contribute to the identification, characterization, and development of new inhibitors toward NDM-1 and its new clinical variants.

METHODS

Protein Expression and Purification

NDM-1 was prepared as described.⁵⁰ Briefly, the NDM-1 gene was cloned into a pET-21a vector. The recombinant NDM-1 protein (residues 36–270) contains a C-terminal His₆-tag (LEHHHHHH) for purification. The protein was expressed in *Escherichia coli* strain BL21 (DE3) cells and purified by Ni^{2+} -affinity chromatography and size exclusion chromatography. For the nonfunctional form, 20 equivalents of EDTA were added to the purified protein. EDTA was soon removed by buffer exchange. Two equivalents of Zn^{2+} were added to the nonfunctional protein to give functional di-Zn-NDM-1. Detailed information can be found in the Supporting Information.

NMR Spectroscopy

TROSY-HNCA, TROSY-HNCO, TROSY-HNCACB, and TROSY-HN(CO)CACB experiments were used to obtain backbone assignments.⁶² NMR titration of ^{15}N -enriched NDM-1 with inhibitors was carried out at 298 K on the Bruker 700, 800, and 850 MHz spectrometers. ^{19}F spectra were acquired at 298 K on a Bruker 600 MHz spectrometer equipped with a 5-mm H/F (C, N) triple resonance cryoprobe. ^{19}F spectra were recorded with spectral widths of 30 ppm with a duty cycle delay of 2.0 s. The numbers of scans of ^{19}F spectra were between 1024 and 2048 depending on the sample concentrations. The concentration of NDM-1 was 0.1–0.3 mM. Detailed information can be found in the Supporting Information.

Thermal Stability Measurement

The circular dichroism data were acquired with a Chirascan spectropolarimeter using quartz cuvettes with a path length of 0.2 cm. The thermal stabilities of NDM-1 and ebselen-bounded NDM-1 were measured by recording the change of ellipticity at 208 nm (θ_{208}) in the temperature range of 25–90 °C with a heating rate of 1 °C/min. The actual temperatures of the sample were acquired through a temperature probe inside the sample.

PCA of Inhibitors' Titration Data

PCA of the inhibitors' titration data by ^1H - ^{15}N TROSY-HSQC was performed by using the method developed by Sakurai and co-workers.⁵⁷ The chemical shift perturbation data from each Zn-NDM-1 titration spectrum were represented as a one-dimensional vector that contains the $\Delta\delta_{\text{H}}$ and $\Delta\delta_{\text{N}}$ values. The $\Delta\delta_{\text{N}}$ values were divided by 8 as a pretreatment. The vectors were utilized to build a two-dimensional matrix \mathbf{X} . In \mathbf{X} , the rows and columns were the chemical shift perturbation data from each spectrum and the variables of the inhibitors, respectively. The matrix size is $246[123 \text{ (number of traceable residues)} \times 2 (\Delta\delta_{\text{H}} \text{ and } \Delta\delta_{\text{N}})] \times 8 \text{ (inhibitors)}$. A standard singular value decomposition analysis was performed on the matrix \mathbf{X} by using the "prcomp" function of the program R.

Isothermal Titration Calorimetry

Isothermal titration calorimetry (ITC) experiments were carried out using a MicroCal VP-ITC instrument (Malvern) with a 1.4 mL cell at 298 K. NDM-1 (40 μM) and inhibitors (500 μM) were dissolved in 50 mM HEPES, 200 mM NaCl, pH 7.5, and degassed before the measurements. The ITC cell was filled with 40 μM NDM-1 (1.4 mL), and NDM-1 solutions were titrated with 259 μL of DTT (500 μM) and tipronin (500 μM) in the presence of 1 mM TCEP over 18 aliquots (the first aliquot was 4 μL and the later aliquot was 17 $\mu\text{L} \times 15 \mu\text{L}$). The reference power and stirring speed were set at 10 $\mu\text{cal/s}$ and 307 g, respectively. The control experiments were conducted by titrating the test inhibitors into a buffer, which showed negligible heat of dilution signals. The peaks were integrated and curves were fitted using MicroCal PEAQ-ITC data analysis software.

ASSOCIATED CONTENT

Supporting Information

The Supporting Information is available free of charge at <https://pubs.acs.org/doi/10.1021/jacsau.2c00651>.

Detailed materials and methods including protein expression and purification; sample preparation; NMR spectroscopy and thermal stability determination (PDF)

Huazhong University of Science and Technology, Wuhan 430074, China; orcid.org/0000-0002-9359-915X

Complete contact information is available at: <https://pubs.acs.org/10.1021/jacsau.2c00651>

AUTHOR INFORMATION

Corresponding Author

Conggang Li – Key Laboratory of Magnetic Resonance in Biological Systems, State Key Laboratory of Magnetic Resonance and Atomic and Molecular Physics, National Center for Magnetic Resonance in Wuhan, Wuhan Institute of Physics and Mathematics, Innovation Academy of Precision Measurement, Chinese Academy of Sciences, Wuhan 430071, China; Wuhan National Laboratory for Optoelectronics, Huazhong University of Science and Technology, Wuhan 430074, China; orcid.org/0000-0002-5798-1722; Email: conggangli@apm.ac.cn

Authors

Kai Cheng – Key Laboratory of Magnetic Resonance in Biological Systems, State Key Laboratory of Magnetic Resonance and Atomic and Molecular Physics, National Center for Magnetic Resonance in Wuhan, Wuhan Institute of Physics and Mathematics, Innovation Academy of Precision Measurement, Chinese Academy of Sciences, Wuhan 430071, China

Qiong Wu – Key Laboratory of Magnetic Resonance in Biological Systems, State Key Laboratory of Magnetic Resonance and Atomic and Molecular Physics, National Center for Magnetic Resonance in Wuhan, Wuhan Institute of Physics and Mathematics, Innovation Academy of Precision Measurement, Chinese Academy of Sciences, Wuhan 430071, China

Chendie Yao – Key Laboratory of Magnetic Resonance in Biological Systems, State Key Laboratory of Magnetic Resonance and Atomic and Molecular Physics, National Center for Magnetic Resonance in Wuhan, Wuhan Institute of Physics and Mathematics, Innovation Academy of Precision Measurement, Chinese Academy of Sciences, Wuhan 430071, China

Zhaofei Chai – Key Laboratory of Magnetic Resonance in Biological Systems, State Key Laboratory of Magnetic Resonance and Atomic and Molecular Physics, National Center for Magnetic Resonance in Wuhan, Wuhan Institute of Physics and Mathematics, Innovation Academy of Precision Measurement, Chinese Academy of Sciences, Wuhan 430071, China

Ling Jiang – Key Laboratory of Magnetic Resonance in Biological Systems, State Key Laboratory of Magnetic Resonance and Atomic and Molecular Physics, National Center for Magnetic Resonance in Wuhan, Wuhan Institute of Physics and Mathematics, Innovation Academy of Precision Measurement, Chinese Academy of Sciences, Wuhan 430071, China; Wuhan National Laboratory for Optoelectronics, Huazhong University of Science and Technology, Wuhan 430074, China

Maili Liu – Key Laboratory of Magnetic Resonance in Biological Systems, State Key Laboratory of Magnetic Resonance and Atomic and Molecular Physics, National Center for Magnetic Resonance in Wuhan, Wuhan Institute of Physics and Mathematics, Innovation Academy of Precision Measurement, Chinese Academy of Sciences, Wuhan 430071, China; Wuhan National Laboratory for Optoelectronics,

Author Contributions

K.C., Q.W., C.Y., F.C., L.J., M.L., and C.L. conceived and designed the experiments. K.C., Q.W., and C.Y. performed the experiments. K.C., Q.W., C.Y., F.C., L.J., M.L., and C.L. analyzed the data. K.C., Q.W., C.Y., L.J., M.L., and C.L. wrote the paper. CRediT: **Kai Cheng** conceptualization, data curation, formal analysis, investigation, validation, writing-original draft, writing-review & editing; **Qiong Wu** data curation, investigation; **Chendie Yao** data curation, formal analysis, investigation, resources, validation, visualization; **Zhaofei Chai** data curation, formal analysis; **Ling Jiang** formal analysis, supervision, validation, visualization; **Maili Liu** supervision, validation, visualization; **Conggang Li** conceptualization, data curation, formal analysis, investigation, supervision, validation, visualization, writing-review & editing.

Notes

The authors declare no competing financial interest.

ACKNOWLEDGMENTS

This work is supported by grants from the National Natural Sciences Foundation of China (21575156, 21925406, and 21904137) and the Ministry of Science and Technology of China (2021YFA1302600).

REFERENCES

- (1) Bush, K. Alarming beta-lactamase-mediated resistance in multidrug-resistant enterobacteriaceae. *Curr. Opin. Microbiol.* **2010**, *13*, 558–564.
- (2) Bush, K.; Jacoby, G. A. Updated functional classification of beta-lactamases. *Antimicrob. Agents Chemother.* **2010**, *54*, 969–976.
- (3) Tondi, D.; Cross, S.; Venturelli, A.; Costi, M. P.; Cruciani, G.; Spyraakis, F. Decoding the structural basis for carbapenem hydrolysis by class A beta-lactamases: fishing for a pharmacophore. *Curr. Drug Targets.* **2016**, *17*, 983–1005.
- (4) Docquier, J. D.; Mangani, S. Structure-function relationships of class D carbapenemases. *Curr. Drug Targets.* **2016**, *17*, 1061–1071.
- (5) Bebrone, C. Metallo-beta-lactamases (classification, activity, genetic organization, structure, zinc coordination) and their superfamily. *Biochem. Pharmacol.* **2007**, *74*, 1686–1701.
- (6) Bonomo, R. A. New Delhi metallo-beta-lactamase and multidrug resistance: a global SOS? *Clin. Infect. Dis.* **2011**, *52*, 485–487.
- (7) Rolain, J. M.; Parola, P.; Cornaglia, G. New Delhi metallo-beta-lactamase (NDM-1): towards a new pandemic? *Clin. Microbiol. Infect.* **2010**, *16*, 1699–1701.
- (8) Nordmann, P.; Poirel, L.; Walsh, T. R.; Livermore, D. M. The emerging NDM carbapenemases. *Trends Microbiol.* **2011**, *19*, 588–595.
- (9) Yong, D.; Toleman, M. A.; Giske, C. G.; Cho, H. S.; Sundman, K.; Lee, K.; Walsh, T. R. Characterization of a new metallo-beta-lactamase Gene, bla(NDM-1), and a novel erythromycin esterase gene carried on a unique genetic structure in klebsiella pneumoniae sequence type 14 from india. *Antimicrob. Agents Chemother.* **2009**, *53*, 5046–5054.
- (10) Papp-Wallace, K. M.; Endimiani, A.; Taracila, M. A.; Bonomo, R. A. Carbapenems: past, present, and future. *Antimicrob. Agents Chemother.* **2011**, *55*, 4943–4960.
- (11) Zhang, H.; Hao, Q. Crystal structure of NDM-1 reveals a common beta-lactam hydrolysis mechanism. *FASEB J.* **2011**, *25*, 2574–2582.

- (12) Yuan, Q.; He, L.; Ke, H. A potential substrate binding conformation of beta-lactams and insight into the broad spectrum of NDM-1 activity. *Antimicrob. Agents Chemother.* **2012**, *56*, 5157–5163.
- (13) Kim, Y.; Tesar, C.; Mire, J.; Jedrzejczak, R.; Binkowski, A.; Babnigg, G.; Sacchettini, J.; et al. Structure of apo- and monometalated forms of NDM-1—a highly potent carbapenem-hydrolyzing metallo-beta-lactamase. *PLoS One* **2011**, *6*, No. e24621.
- (14) King, D.; Strynadka, N. Crystal structure of New Delhi metallo-beta-lactamase reveals molecular basis for antibiotic resistance. *Protein Sci.* **2011**, *20*, 1484–1491.
- (15) Kim, Y.; Cunningham, M. A.; Mire, J.; Tesar, C.; Sacchettini, J.; Joachimiak, A. NDM-1, the ultimate promiscuous enzyme: substrate recognition and catalytic mechanism. *FASEB J.* **2013**, *27*, 1917–1927.
- (16) Aitha, M.; Moller, A. J.; Sahu, I. D.; Horitani, M.; Tierney, D. L.; Crowder, M. W. Investigating the position of the hairpin loop in New Delhi metallo-beta-lactamase, NDM-1, during catalysis and inhibitor binding. *J. Inorg. Biochem.* **2016**, *156*, 35–39.
- (17) Drawz, S. M.; Bonomo, R. A. Three decades of beta-lactamase inhibitors. *Clin. Microbiol. Rev.* **2010**, *23*, 160–201.
- (18) Eidam, O.; Romagnoli, C.; Dalmaso, G.; Barelier, S.; Caselli, E.; Bonnet, R.; Shoichet, B. K.; et al. Fragment-guided design of subnanomolar beta-lactamase inhibitors active in vivo. *Proc. Natl. Acad. Sci. U.S.A.* **2012**, *109*, 17448–17453.
- (19) Tondi, D.; Venturelli, A.; Bonnet, R.; Pozzi, C.; Shoichet, B. K.; Costi, M. P. Targeting class A and C serine beta-lactamases with a broad-spectrum boronic acid derivative. *J. Med. Chem.* **2014**, *57*, 5449–5458.
- (20) Genovesi, F.; Lazzari, S.; Venturi, E.; Costantino, L.; Blazquez, J.; Ibacache-Quiroga, C.; Costi, M.; et al. Design, synthesis and biological evaluation of non-covalent AmpC beta-lactamase inhibitors. *Med. Chem. Res.* **2017**, *26*, 975–986.
- (21) van den Akker, F.; Bonomo, R. A. Exploring additional dimensions of complexity in inhibitor design for serine β -lactamases: mechanistic and intra- and inter-molecular chemistry approaches. *Front Microbiol.* **2018**, *9*, 622.
- (22) Celenza, G.; Vicario, M.; Bellio, P.; Linciano, P.; Perilli, M.; Oliver, A.; Blazquez, J.; et al. Phenylboronic acid derivatives as validated leads active in clinical strains overexpressing KPC-2: a step against bacterial resistance. *Chemmedchem* **2018**, *13*, 713–724.
- (23) Linciano, P.; Cendron, L.; Gianquinto, E.; Spyarakis, F.; Tondi, D. Ten years with New Delhi metallo-beta-lactamase-1 (NDM-1): from structural insights to inhibitor design. *ACS Infect. Dis.* **2019**, *5*, 9–34.
- (24) Wang, T.; Xu, K. J.; Zhao, L. Y.; Tong, R. S.; Xiong, L.; Shi, J. Y. Recent research and development of NDM-1 inhibitors. *Eur. J. Med. Chem.* **2021**, *223*, No. 113667.
- (25) Gu, X. X.; Zheng, M. Z.; Chen, L. X.; Li, H. The development of New Delhi metallo-beta-lactamase-1 inhibitors since 2018. *Microbiol. Res.* **2022**, *261*, No. 127079.
- (26) King, A. M.; Reid-Yu, S. A.; Wang, W. L.; King, D. T.; De Pascale, G.; Strynadka, N. C.; Walsh, T. R.; et al. Aspergillomarasmine A overcomes metallo-beta-lactamase antibiotic resistance. *Nature* **2014**, *510*, 503–506.
- (27) Sun, H. Z.; Zhang, Q.; Wang, R. M.; Wang, H. B.; Wong, Y. T.; Wang, M. J.; Hao, Q.; et al. Resensitizing carbapenem- and colistin-resistant bacteria to antibiotics using auranofin. *Nat. Commun.* **2020**, *11*, No. 5263.
- (28) Wang, R. M.; Lai, T. P.; Gao, P.; Zhang, H. M.; Ho, P. L.; Woo, P. C. Y.; Ma, G. X.; et al. Bismuth antimicrobial drugs serve as broad-spectrum metallo-beta-lactamase inhibitors. *Nat. Commun.* **2018**, *9*, No. 439.
- (29) Yusof, Y.; Tan, D. T. C.; Arjomandi, O. K.; Schenk, G.; McGeary, R. P. Captopril analogues as metallo-beta-lactamase inhibitors. *Bioorg. Med. Chem. Lett.* **2016**, *26*, 1589–1593.
- (30) Klingler, F. M.; Wichelhaus, T. A.; Frank, D.; Cuesta-Bernal, J.; El-Delik, J.; Muller, H. F.; Sjuts, H.; et al. Approved drugs containing thiols as inhibitors of metallo-beta-lactamases: strategy to combat multidrug-resistant bacteria. *J. Med. Chem.* **2015**, *58*, 3626–3630.
- (31) Brem, J.; Cain, R.; Cahill, S.; McDonough, M. A.; Clifton, I. J.; Jimenez-Castellanos, J. C.; Avison, M. B.; et al. Structural basis of metallo-beta-lactamase, serine-beta-lactamase and penicillin-binding protein inhibition by cyclic boronates. *Nat. Commun.* **2016**, *7*, No. 12406.
- (32) Chiou, J. C.; Wan, S. B.; Chan, K. F.; So, P. K.; He, D. D.; Chan, E. W. C.; Chan, T. H.; et al. Ebselen as a potent covalent inhibitor of New Delhi metallo-beta-lactamase (NDM-1). *Chem. Commun.* **2015**, *51*, 9543–9546.
- (33) Thomas, P. W.; Spicer, T.; Cammarata, M.; Brodbelt, J. S.; Hodder, P.; Fast, W. An altered zinc-binding site confers resistance to a covalent inactivator of New Delhi metallo-beta-lactamase-1 (NDM-1) discovered by high-throughput screening. *Bioorg. Med. Chem.* **2013**, *21*, 3138–3146.
- (34) Naas, T.; Oueslati, S.; Bonnin, R. A.; Dabos, M. L.; Zavala, A.; Dortet, L.; Retailleau, P.; Iorga, B. I. Beta-lactamase database (BLDB) - structure and function. *J. Enzyme Inhib. Med. Chem.* **2017**, *32*, 917–919.
- (35) Stewart, A. C.; Bethel, C. R.; VanPelt, J.; Bergstrom, A.; Cheng, Z. S.; Miller, C. G.; Williams, C.; et al. Clinical variants of New Delhi metallo-beta-lactamase are evolving to overcome zinc scarcity. *ACS Infect. Dis.* **2017**, *3*, 927–940.
- (36) Farhat, N.; Khan, A. U. Evolving trends of New Delhi metallo-beta-lactamase (NDM) variants: a threat to antimicrobial resistance. *Infect., Genet. Evol.* **2020**, *86*, No. 104588.
- (37) Clore, G. M.; Gronenborn, A. M. Theory and applications of the transferred nuclear overhauser effect to the study of the conformations of small ligands bound to proteins. *J. Magn. Reson.* **1982**, *48*, 402–417.
- (38) Ni, F.; Scheraga, H. A. Use of the transferred nuclear overhauser effect to determine the conformations of ligands bound to proteins. *Acc. Chem. Res.* **1994**, *27*, 257–264.
- (39) Mayer, M.; Meyer, B. Characterization of ligand binding by saturation transfer difference NMR spectroscopy. *Angew. Chem., Int. Ed.* **1999**, *38*, 1784–1788.
- (40) Dalvit, C.; Pevarello, P.; Tato, M.; Veronesi, M.; Vulpetti, A.; Sundstrom, M. Identification of compounds with binding affinity to proteins via magnetization transfer from bulk water. *J. Biomol. NMR* **2000**, *18*, 65–68.
- (41) Dalvit, C.; Fogliatto, G.; Stewart, A.; Veronesi, M.; Stockman, B. WaterLOGSY as a method for primary NMR screening: practical aspects and range of applicability. *J. Biomol. NMR* **2001**, *21*, 349–359.
- (42) Mayer, M.; Meyer, B. Group epitope mapping by saturation transfer difference NMR to identify segments of a ligand in direct contact with a protein receptor. *J. Am. Chem. Soc.* **2001**, *123*, 6108–6117.
- (43) Meyer, B.; Peters, T. NMR spectroscopy techniques for screening and identifying ligand binding to protein receptors. *Angew. Chem., Int. Ed.* **2003**, *42*, 864–890.
- (44) Constantine, K. L.; Davis, M. E.; Metzler, W. J.; Mueller, L.; Claus, B. L. Protein-ligand NOE matching: a high-throughput method for binding pose evaluation that does not require protein NMR resonance assignments. *J. Am. Chem. Soc.* **2006**, *128*, 7252–7263.
- (45) Caburet, J.; Boucherle, B.; Bourdillon, S.; Simoncelli, G.; Verdirosa, F.; Docquier, J. D.; Moreau, Y.; et al. A fragment-based drug discovery strategy applied to the identification of NDM-1 beta-lactamase inhibitors. *Eur. J. Med. Chem.* **2022**, *240*, No. 114599.
- (46) Rydzik, A. M.; Brem, J.; van Berkel, S. S.; Pfeffer, I.; Makena, A.; Claridge, T. D. W.; Schofield, C. J. Monitoring conformational changes in the NDM-1 metallo-beta-lactamase by ^{19}F NMR spectroscopy. *Angew. Chem., Int. Ed.* **2014**, *53*, 3129–3133.
- (47) Rydzik, A. M.; Brem, J.; Chandler, S. A.; Benesch, J. L. P.; Claridge, T. D. W.; Schofield, C. J. Monitoring protein-metal binding by ^{19}F NMR - a case study with the New Delhi metallo-beta-lactamase 1. *RSC Med. Chem.* **2020**, *11*, 387–391.
- (48) Riviere, G.; Oueslati, S.; Gayral, M.; Crechet, J. B.; Nhiri, N.; Jacquet, E.; Cintrat, J. C.; et al. NMR characterization of the influence of zinc(II) ions on the structural and dynamic behavior of the New

Delhi metallo-beta-lactamase-1 and on the binding with flavonols as inhibitors. *ACS Omega* **2020**, *5*, 10466–10480.

(49) Palica, K.; Voracova, M.; Skagseth, S.; Rasmussen, A. A.; Allander, L.; Hubert, M.; Sandegren, L.; et al. Metallo-beta-lactamase inhibitor phosphoramidate monoesters. *ACS Omega* **2022**, *7*, 4550–4562.

(50) Yao, C.; Wu, Q.; Xu, G.; Li, C. NMR backbone resonance assignment of New Delhi metallo-beta-lactamase. *Biomol. NMR Assign* **2017**, *11*, 239–242.

(51) Chen, A. L. Y.; Thomas, P. W.; Stewart, A. C.; Bergstrom, A.; Cheng, Z. S.; Miller, C.; Bethel, C. R.; et al. Dipicolinic acid derivatives as inhibitors of New Delhi metallo-beta-lactamase-1. *J. Med. Chem.* **2017**, *60*, 7267–7283.

(52) Schnaars, C.; Kildahl-Andersen, G.; Prandina, A.; Popal, R.; Radix, S.; Le Borgne, M.; Gjoen, T.; et al. Synthesis and preclinical evaluation of TPA-based zinc chelators as metallo-beta-lactamase inhibitors. *ACS Infect. Dis.* **2018**, *4*, 1407–1422.

(53) Li, N. N.; Xu, Y. T.; Xia, Q.; Bai, C. G.; Wang, T. Y.; Wang, L.; He, D. D.; et al. Simplified captopril analogues as NDM-1 inhibitors. *Bioorg. Med. Chem. Lett.* **2014**, *24*, 386–389.

(54) Yang, Y. J.; Bush, K. Biochemical characterization of the carbapenem-hydrolyzing beta-lactamase AsbM1 from *Aeromonas sobria* AER 14M: a member of a novel subgroup of metallo-beta-lactamases. *FEMS Microbiol. Lett.* **1996**, *137*, 193–200.

(55) Day, T. A.; Chen, G. Z. The metalloprotease inhibitor 1,10-phenanthroline affects *Schistosoma mansoni* motor activity, egg laying and viability. *Parasitology* **1998**, *116*, 319–325.

(56) Thomas, P. W.; Cammarata, M.; Brodbelt, J. S.; Fast, W. Covalent inhibition of New Delhi metallo-beta-lactamase-1 (NDM-1) by cefaclor. *ChemBioChem* **2014**, *15*, 2541–2548.

(57) Sakurai, K.; Goto, Y. Principal component analysis of the pH-dependent conformational transitions of bovine beta-lactoglobulin monitored by heteronuclear NMR. *Proc. Natl. Acad. Sci. U.S.A.* **2007**, *104*, 15346–15351.

(58) King, D. T.; Worrall, L. J.; Gruninger, R.; Strynadka, N. C. J. New Delhi metallo-beta-lactamase: structural insights into beta-lactam recognition and inhibition. *J. Am. Chem. Soc.* **2012**, *134*, 11362–11365.

(59) Brem, J.; Panduwawala, T.; Hansen, J. U.; Hewitt, J.; Liepins, E.; Donets, P.; Espina, L.; et al. Imitation of beta-lactam binding enables broad-spectrum metallo-beta-lactamase inhibitors. *Nat. Chem.* **2022**, *14*, 15–22.

(60) Guo, H.; Cheng, K.; Gao, Y.; Bai, W.; Wu, C.; He, W.; Li, C.; Li, Z. A novel potent metal-binding NDM-1 inhibitor was identified by fragment virtual, SPR and NMR screening. *Bioorg. Med. Chem.* **2020**, *28*, No. 115437.

(61) Ma, J.; McLeod, S.; MacCormack, K.; Sriram, S.; Gao, N.; Breeze, A. L.; Hu, J. Real-time monitoring of New Delhi metallo-beta-lactamase activity in living bacterial cells by ^1H NMR spectroscopy. *Angew. Chem., Int. Ed.* **2014**, *53*, 2130–2133.

(62) Salzmann, M.; Pervushin, K.; Wider, G.; Senn, H.; Wuthrich, K. TROSY in triple-resonance experiments: new perspectives for sequential NMR assignment of large proteins. *Proc. Natl. Acad. Sci. U.S.A.* **1998**, *95*, 13585–13590.